Phase selection and nanocrystallization in Cu-free soft magnetic FeSiNbB amorphous alloy upon rapid annealing

L. Morsdorf, K. G. Pradeep' , G. Herzer, A. Kovács, R. E. Dunin-Borkowski, I. Povstugar, G. Konygin, P. Choi, and D. Raabe

Citation: J. Appl. Phys. **119**, 124903 (2016); doi: 10.1063/1.4944595
View online: http://dx.doi.org/10.1063/1.4944595
View Table of Contents: http://aip.scitation.org/toc/jap/119/12
Published by the American Institute of Physics

Articles you may be interested in

Investigation on the crystallization mechanism difference between FINEMET® and NANOMET® type Fe-based soft magnetic amorphous alloys
J. Appl. Phys. **120**, 145102145102 (2016); 10.1063/1.4964433

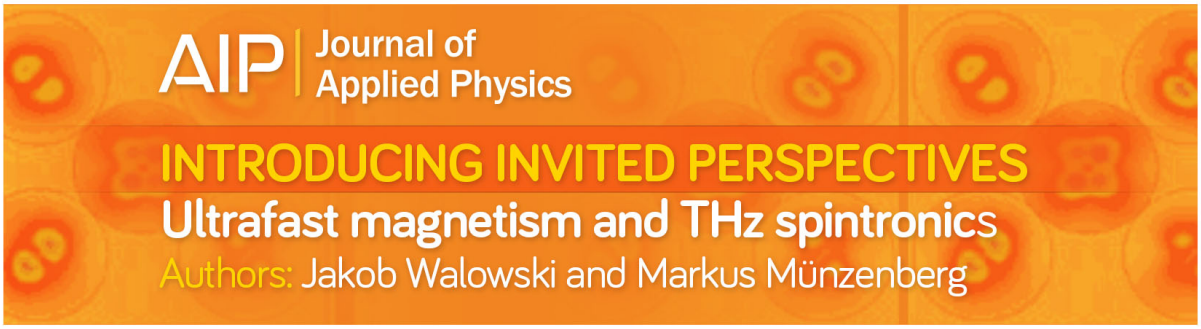

RIGHTSLINK

Phase selection and nanocrystallization in Cu-free soft magnetic FeSiNbB amorphous alloy upon rapid annealing

L. Morsdorf,[1] K. G. Pradeep,[1,2,a)] G. Herzer,[3] A. Kovács,[4] R. E. Dunin-Borkowski,[4] I. Povstugar,[1] G. Konygin,[5] P. Choi,[6] and D. Raabe[1]
[1]*Department for Microstructure Physics and Alloy Design, Max-Planck-Institut für Eisenforschung GmbH, Max-Planck-Str. 1, 40237 Düsseldorf, Germany*
[2]*Materials Chemistry, RWTH Aachen University, Kopernikusstrasse 10, 52074 Aachen, Germany*
[3]*Vacuumschmelze GmbH & Co KG, Grüner Weg 37, D-63450 Hanau, Germany*
[4]*Ernst Ruska-Centre for Microscopy and Spectroscopy with Electrons and Peter Grünberg Institute 5, Forschungszentrum Jülich, 52425 Jülich, Germany*
[5]*Physical-Technical Institute UrB RAS, Kirov str. 132, 426008 Izhevsk, Russia*
[6]*Department of Materials Science and Engineering, Korea Advanced Institute of Science and Technology, Daejeon 34141, Korea*

(Received 4 January 2016; accepted 8 March 2016; published online 24 March 2016)

Nucleation of soft magnetic Fe_3Si nanocrystals in Cu-free $Fe_{74.5}Si_{15.5}Nb_3B_7$ alloy, upon rapid (10 s) and conventional (30 min) annealing, was investigated using x-ray diffraction, transmission electron microscopy, Mössbauer spectroscopy, and atom probe tomography. By employing rapid annealing, preferential nucleation of Fe_3Si nanocrystals was achieved, whereas otherwise there is simultaneous nucleation of both Fe_3Si and undesired Fe-B compound phases. Analysis revealed that the enhanced Nb diffusivity, achieved during rapid annealing, facilitates homogeneous nucleation of Fe_3Si nanocrystals while shifting the secondary Fe-B crystallization to higher temperatures resulting in pure soft magnetic nanocrystallization with very low coercivities of ~10 A/m. © *2016 AIP Publishing LLC*. [http://dx.doi.org/10.1063/1.4944595]

I. INTRODUCTION

Partially nanocrystalline Fe-Si-B based amorphous alloys are known to exhibit excellent soft magnetic properties.[1] As introduced by Yoshizawa *et al.*,[2] small additions of Cu and Nb facilitate the formation of an amorphous-crystalline nanocomposite microstructure upon annealing of initially amorphous precursor materials. In the case of FINEMET type ($Fe_{73.5}Si_{13.5}Nb_3B_9Cu_1$, $Fe_{73.5}Si_{15.5}Nb_3B_7Cu_1$) alloys, optimum nanostructures are obtained after conventional annealing (CA) for ~30–60 min at temperatures slightly higher than the onset temperature of primary crystallization (~570 °C).[3] The resulting nanocomposite microstructure is characterized by the presence of soft-magnetic Fe_3Si nanocrystals (70–80 vol. %) having a size of 15–20 nm embedded in the remaining amorphous matrix.[4–6] In this regime of nano-sized crystals, optimum soft magnetic properties including very low coercivity values and negligible saturation magnetostriction are obtained.[3]

Recently, rapid annealing (RA) of amorphous $Fe_{73.5}Si_{15.5}Nb_3B_7Cu_1$ alloys was introduced, wherein the amorphous precursor materials were annealed at temperatures higher than that required for CA by at least ~100 °C for very short annealing times of 4–10 s.[5,7] Such a procedure also resulted in similar nanocrystalline microstructures comparable to those of their CA counterparts.[5] The underlying reason for obtaining such similar nanostructures, even though the annealing procedures are very different, is attributed to the presence of 1 at. % Cu. It was observed using atom probe tomography (APT) that the clustering of Cu atoms upon RA starts prior to the onset of primary crystallization, thereby introducing chemical heterogeneities in the amorphous matrix. Such local chemical heterogeneities include Fe-Si rich regions (acting as nuclei) which at higher annealing temperatures nucleate into DO_3 structured Fe_3Si nanocrystals. In addition to the well-established Cu clustering induced heterogeneous nucleation mechanism of Fe_3Si nanocrystals proposed by Hono *et al.*,[4,8] the recently observed chemical heterogeneity induced nucleation during RA has introduced a novel way of obtaining ultra-fine-grained nanocrystals (10–12 nm) with high number density. The usefulness of such a RA process is shown by the case of the newly developed Fe-rich (>80 at. %) NANOMET alloys, where uniform nanocrystalline (<20 nm) microstructures with outstanding soft magnetic properties are achieved by RA.[9]

Having realized the potential of RA for nanocrystallization, we investigate in this study the effect of RA on the soft magnetic Fe_3Si nanocrystallization in Cu-free $Fe_{74.5}Si_{15.5}Nb_3B_7$ alloy. It has been reported that the Cu-free $Fe_{74.5}Si_{15.5}Nb_3B_7$ alloy undergoes simultaneous nucleation of both soft-magnetic Fe_3Si phase and undesired hard-magnetic Fe-B compounds upon CA. Hence, the objective of this study is two-fold: First, we explore the possibility of obtaining isolated soft-magnetic Fe_3Si nanocrystals employing RA, as observed in the case of $Fe_{73.5}Si_{15.5}Nb_3B_7Cu_1$ alloy. Second, the RA induced nanocrystallization process is utilized to understand the atomic-scale mechanisms during homogeneous nucleation Fe_3Si nanocrystals.

II. EXPERIMENTAL PROCEDURE

Amorphous $Fe_{74.5}Si_{15.5}Nb_3B_7$ (at. %) precursor ribbons were prepared by rapid solidification from the melt on a rotating water-cooled Cu wheel in an Ar atmosphere. The

a)Author to whom correspondence should be addressed. Electronic addresses: kg.prad@mpie.de and kgprad@gmail.com

 © 2016 AIP Publishing LLC

RIGHTSLINK

as-produced ribbons were ~5 mm in width and 20–30 μm in thickness. Thermal stability and phase formation in the amorphous ribbon were studied using differential scanning calorimetry (DSC) employing a NETZSCH Pegasus 404 C instrument at 20 K/min heating rate. Partial nanocrystallization was achieved by annealing the as-spun amorphous ribbon at different temperatures by two different methods, namely, RA (10 s) and CA (30 min).[5] RA was performed utilizing a highly conductive Cu block which was pre-heated in the furnace for a minimum duration of 15 min at the set temperature. The as-prepared amorphous ribbons were introduced into the center of the block by means of a pre-heated Cu drawer (sliding plate carrying ribbons). After holding at the set temperature for 10 s, the Cu drawer carrying the ribbons were immediately ejected from the Cu blocks. Since the ribbons had a limited thickness of 20–30 μm, they get rapidly cooled to the room temperature ($\leq$1–2 s) upon exiting the furnace. Multiple annealing trails were performed to ensure reproducibility.

X-ray diffraction patterns were recorded in the 2θ range of 20°–120° using a SEIFERT type ID3003 X-ray generator with Co $K\alpha 1$ radiation ($\lambda = 0.178$ nm) and a HUBER 2-circle goniometer with a Meteor0D detector. Nanostructure analyses including bright field (BF) imaging and selected area diffraction patterns (SAD) were carried out by transmission electron microscopy (TEM) using a PHILIPS CM 20 microscope operated at 200 kV. The average size of the nanocrystals was estimated from a series of BF images including a minimum of 100 grains. In order to understand the influence of grain size and phases formed on the magnetic microstructure, magnetic domain walls (DWs) were imaged in magnetic field free conditions by recording defocused Fresnel images using a FEI TITAN 60–300 microscope operated at 300 kV. ^{57}Fe Mössbauer spectra were measured at room temperature using a spectrometer with a ^{57}Co(Cr) source operating in constant acceleration mode. A generalizing regular algorithm for the solution of the inversion problem was used to restore the hyperfine field distribution functions P(H) from the spectra.[10] Elemental distributions on a near-atomic scale were investigated by APT using a Local Electrode Atom Probe (LEAP^{TM} 3000X HR, CAMECA Instruments) maintained under ultrahigh vacuum conditions (~10^{-11} Torr). The pulse fraction and pulse repetition rate were 15% and 200 kHz, respectively. The tip temperature was maintained at 60 K. The acquired data were analyzed using the IVAS 3.6.6 software supplied by CAMECA Inc. Needle-shaped samples for APT investigations and TEM lamellae were prepared using a HELIOS Nanolab 600i dual beam focused ion beam system (FIB). Magnetic hysteresis data were obtained using a BROCKHAUS MPG 100D instrument operated in the AC mode.

III. RESULTS AND DISCUSSION

The XRD patterns of RA and CA samples are shown for various annealing temperatures around peak crystallization in Figs. 1(a) and 1(b). Broad diffraction peaks, characteristic of the amorphous phase are visible for the as-prepared ribbons. The onset of crystallization was observed at 610 °C for RA and at 540 °C for CA, respectively. For the case of RA, the onset of crystallization was characterized by the emergence of the {2 2 0} Fe_3Si peak (marked by an arrow in Fig. 1(a)). In contrast, during CA, the initial amorphous peak develops into a plateau-like dual phase peak (marked by an arrow in Fig. 1(b)). This indicates the simultaneous nucleation of both Fe_3Si phase and Fe-B compounds upon CA which is in good agreement with the observed single-exothermic peak of DSC (Fig. 1(c)) indicating a single crystallization event. The DSC results also reveal that addition of 1 at. % Cu results in a two-step crystallization process where the crystallization of soft magnetic Fe_3Si phase precedes Fe-B compound formation. However, the XRD pattern of the 610 °C RA sample surprisingly indicates the presence of only Fe_3Si phase without any evidence of Fe-B compound formation.

The BF TEM image of the 610 °C RA sample in Fig. 2(a) shows the presence of 13.5 ± 2 nm sized crystals well-separated from each other by the residual amorphous matrix. The SAD pattern (inset of Fig. 2(a)) shows the presence of a typical amorphous halo ring pattern with discrete diffraction spots corresponding to {2 2 0}, {4 0 0}, and {4 2 2} reflections confirming the presence of only the DO_3 structured Fe_3Si soft-magnetic phase. The number density of nanocrystals as estimated from a series of BF TEM images assuming a uniform lamella thickness yields ~3×10^{23} m^{-3} with ~40% crystalline volume fraction. In contrast, CA at 540 °C resulted in the formation of large sized (22.5 ± 4 nm) nanocrystals (the images of which are not shown here) having a relatively low number density of ~8×10^{21} m^{-3} and correspondingly a low volume fraction of only ~5%. Increasing the RA temperature to 620 °C resulted in the crystallization

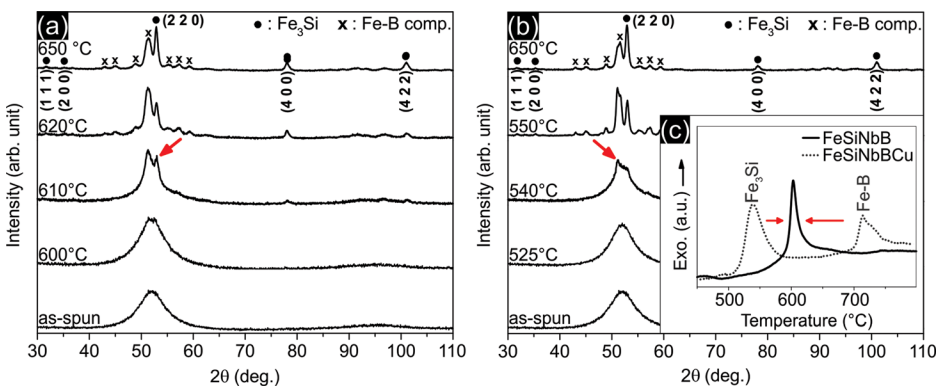

FIG. 1. XRD patterns of $Fe_{74.5}Si_{15.5}Nb_3B_7$ (a) rapid annealed (RA, 10 s) and (b) conventionally annealed (CA, 30 min) at different temperatures; (c) DSC curves of $Fe_{74.5}Si_{15.5}Nb_3B_7$ and $Fe_{73.5}Si_{15.5}Nb_3B_7Cu_1$ amorphous samples obtained at 20 K/min heating rate.

RIGHTSLINK

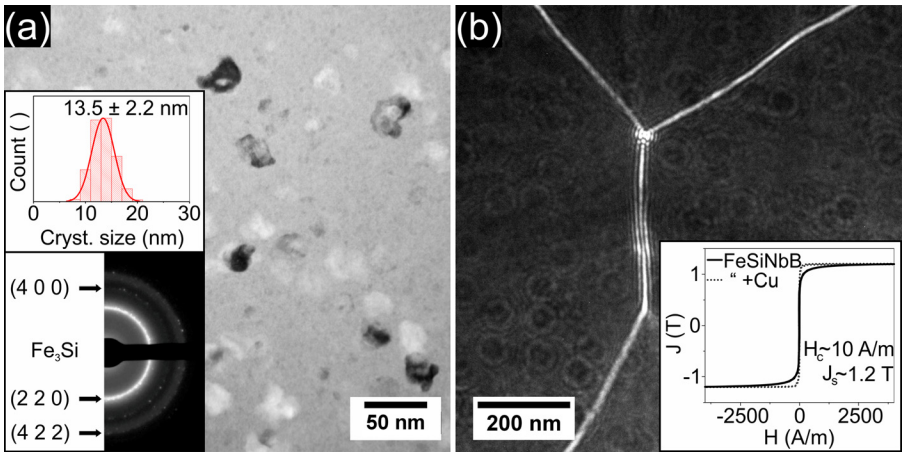

FIG. 2. (a) BF TEM image of the 610 °C RA sample with top inset showing the crystallite size histogram and bottom inset showing SAD analysis; (b) Fresnel image recorded at 400 μm defocus showing large magnetic domains separated by domain walls (white contrast lines). Inset is magnetic hysteresis curves of RA $Fe_{74.5}Si_{15.5}Nb_3B_7$ sample in comparison to RA $Fe_{73.5}Si_{15.5}Nb_3B_7Cu_1$ sample, each with optimum heat treatment.

of Fe-B compound phases as indicated by the corresponding XRD pattern showing multiple low intensity diffraction peaks, which become more prominent after annealing at 650 °C (Fig. 1(a)). The magnetic domain structure of the 610 °C RA sample contains randomly distributed μm-sized domains separated with DW as shown in Fig. 2(b). The magnetic DWs shows no indication of pinning at amorphous-crystalline interfaces or by second phase particles.[11] The observed network of magnetic domains is characteristic of a true soft-magnetic material showing wide individual domains spreading over a large number of Fe_3Si nanocrystals.[12] In view of the random anisotropy model,[3] it is obvious that the magnetic moments of neighboring Fe_3Si nanocrystals are indeed strongly coupled (regardless of their individual orientations) instead of being separated into fine domain network. Hence, the local magnetic moments are enabled to align easily to the applied external magnetic field resulting in highly reduced coercive values of ~10 A/m (inset of Fig. 2(b)) comparable to that of Cu containing alloys.

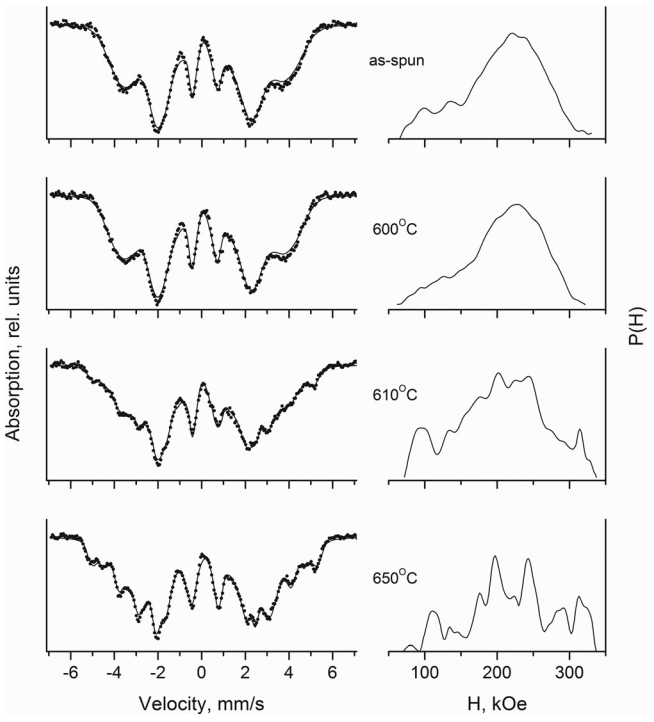

FIG. 3. Mössbauer spectra and corresponding hyperfine magnetic field distributions for as-spun and RA (10 s) samples.

Formation of only Fe_3Si crystalline phase in the amorphous matrix after RA at 610 °C is also confirmed by Mössbauer spectroscopy measurements (Fig. 3). The ^{57}Fe Mössbauer spectra for the as-spun and 600 °C RA samples (10 s) are typical of amorphous phase. A broad halo in the hyperfine magnetic field distribution P(H) can be observed for these samples, with no discernable contributions from field components characteristic of any crystalline phases. The first changes are observed after RA at 610 °C, where two peaks at ~200 and 315 kOe characteristic of Fe_3Si intermetallic phase[13,14] emerge in the P(H) distribution over the broad amorphous halo. Another peak can be observed at ~245 kOe, which is absent in Mössbauer spectra of stoichiometric Fe_3Si but emerge in case of Si deficiency,[13] indicating that Fe_3Si crystallized with Si concentration slightly below 25 at. %. With increasing annealing temperature, the field components of Fe_3Si raise in intensity indicating the increase in phase fraction. However, a halo component is still present in the P(H) distribution even for the 650 °C RA sample, evidence that a significant fraction of the Fe atoms still exhibits local atomic surroundings characteristic of an amorphous phase. Fe_3Si crystallites are obviously non-stoichiometric at this temperature, as indicated by the presence of an intensive peak at 245 kOe.

In order to understand the mechanism of RA enabled preferential Fe_3Si nanocrystallization and hence the influence of individual elements on the nucleation mechanism, APT measurements were carried out on the RA (610 °C) and CA (550 °C) samples annealed at the onset of crystallization for both conditions. Elemental maps with atomic positions of Si, B and Nb are shown also in terms of their iso-concentration surfaces (for clarity) using 21 at. % Si and 6 at. % Nb as the threshold values in Figs. 4(a1) and 4(b1), for RA and CA conditions, respectively.

Both reconstructed volumes of the RA and the CA samples contain well-separated Si-rich regions supposedly corresponding to the Fe_3Si nanocrystals. Proximity analysis of these regions (indicated by dotted rectangles) in Figs. 4(a2) and 4(b2) further confirms that the Si-rich region could well correspond to Fe_3Si nanocrystals containing approximately 23 at. % Si. This observation is in excellent accordance with the

RIGHTSLINK

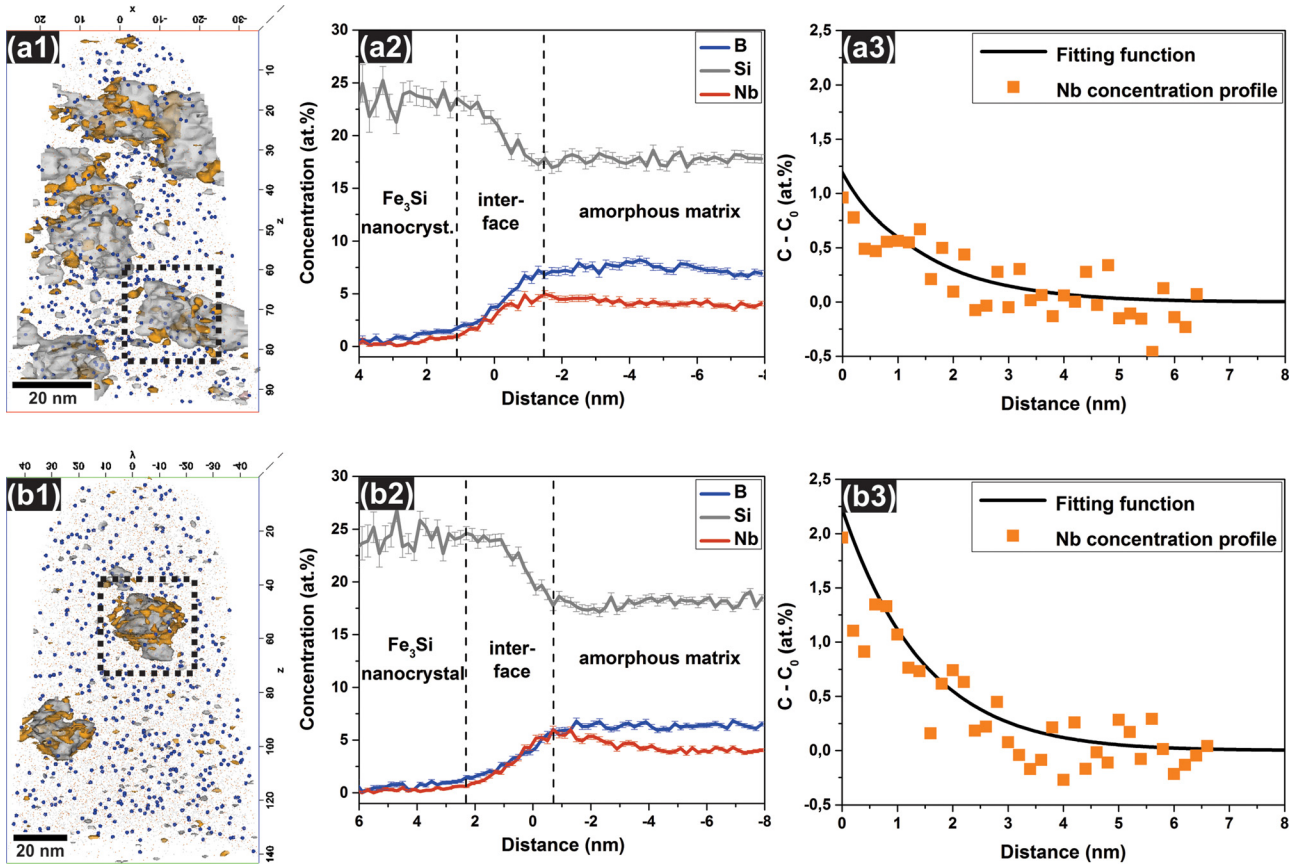

FIG. 4. Reconstructed volume from APT measurement of (a1) RA (10 s) sample at 610 °C and (b1) CA (5 min) sample at 550 °C applying 21 at. % (●) Si and 6 at. % (●)Nb iso-concentration surfaces. (a2), (b2) Proximity analysis of marked Si iso-concentration surface with 0.2 nm bin size; (a3), (b3) Nb diffusion analysis as per the diffusion model.[16] Reproduced with permission from K. G. Pradeep, Ph.D. Dissertation, Shaker Verlag GmbH, 2014. ISBN: 978-3-8440-3211-6.[22]

previous reports on the chemical composition of such Fe_3Si nanocrystals.[5,15] However, a careful inspection of the proximity histogram shows a slight deficiency of Si (by 1–2 at. %) compared to the stoichiometric Fe:Si ratio, being in a good agreement with the Mössbauer spectroscopy results. Additionally, both B and Nb are partitioned out of the Si-rich regions with the concentration of B gradually increasing towards the amorphous matrix, while Nb piles-up at the crystalline-amorphous interface (see Figs. 4(a2) and 4(b2)). The maximum Nb concentrations in the interface region were ~4.9 at. % for the RA sample and ~6 at. % for the CA sample.

It becomes obvious that the larger atomic sized Nb atoms act as a chemical barrier for the nucleation and growth of Fe_3Si nanocrystals which is further controlled by the diffusion of piled-up Nb into the rest amorphous matrix. In theory, the resulting diffusion fields can be described by the solution to the moving boundary problem developed by Frank.[16] Such a solution is ideally applicable for the growth of precipitates in an infinite matrix controlled by the diffusion of one solute. The suitability of this solution has already been demonstrated in the case of Al-Y-Fe metallic glass where pure Al nanocrystals nucleate during primary crystallization and their growth rate is controlled by the diffusion of piled-up Y at the interface.[17,18] Similarly, the gradual decrease of Nb concentration (C) from the pile-up at the interface towards the amorphous matrix (C_0) can therefore be approximated with

$$C - C_0 = \frac{1}{2}(C_m - C_p)S^3 \exp\left(\frac{S^4}{4}\right) \times \left[s^{-1}\exp\left(-\frac{s^2}{4} - \frac{\sqrt{\pi}}{2}erfc\left(\frac{s}{2}\right)\right)\right],$$

where $s = \frac{r}{\sqrt{Dt}}$ with r being the radius of interest ahead of the piled-up interface, D is the diffusion coefficient of Nb, $S = \frac{R}{\sqrt{Dt}}$ with R being the crystallite size (obtained from TEM BF images), and t the corresponding growth time (estimated by taking into account the average crystallite size and the annealing time).[16–18] C_m and C_p are the concentrations of Nb in the matrix and in the particle, respectively, as determined from the APT analyses (Figs. 4(a2) and 4(b2)). Considering the fact that the onset of crystallization stage is investigated using APT, there are no overlaps between the diffusion profiles of neighboring crystals, and hence the validity of the above equation is maintained. The experimentally observed Nb concentration profiles were then subjected to a best fit using the above described diffusion model in order to estimate the diffusion coefficient of Nb under RA and CA conditions as shown in Figs. 4(a3) and 4(b3). Accordingly, the Nb diffusion coefficient for RA yields $\sim 1 \times 10^{-17}$ m^2/s and $\sim 1 \times 10^{-19}$ m^2/s for CA. Thus, the diffusion of Nb in the amorphous matrix is enhanced by about two orders of magnitude upon RA. The increase of the Nb mobility during RA is achieved mainly because of using elevated temperature

RIGHTSLINK

(atleast by 100 °C) annealing compared to CA. The estimated Nb diffusivity during RA is atleast three orders of magnitude higher than those reported for Nb volume diffusion in α-Fe at 500 °C.[19] It is therefore obvious that homogeneous nucleation of Fe_3Si nanocrystals occurs during RA, once Nb has diffused out from the local Fe and Si-rich (nuclei) regions in the amorphous matrix. Hence, it can be generally inferred that homogeneous primary Fe-Si nanocrystallization is possible during RA, provided the existence of favorable local chemical heterogeneities in the amorphous matrix, either as quenched-in nuclei or induced by the addition of minor alloying elements like Cu or Au.[5,20] In the case of Cu addition (∼1 at. %), a maximum crystalline fraction of ∼80 vol. % can be achieved compared to ∼40 vol. % in the present Cu-free case. This is because Cu atoms start clustering prior to the onset of primary crystallization inducing a high density of chemical heterogeneities in the amorphous matrix.[4,5] In addition, the Cu-rich clusters themselves act as heterogeneous nucleation sites for Fe_3Si nanocrystallization. The combination of both these effects results in higher volume fractions of Fe_3Si nanocrystals.[5] Irrespective of the role of Cu, the observed primary homogeneous nucleation of Fe_3Si nanocrystals in the Cu-free alloy has validated the reported chemical fluctuation induced nanocrystallization mechanism suggested for RA.[5]

The preferential nucleation of Fe_3Si nanocrystals without the formation of Fe-B compounds during RA can be explained by the fact that Nb increases the thermal stability of the amorphous matrix.[20,21] Having realized that the mobility of Nb atoms is significantly increased during RA, the Nb atoms piling up at the interfaces of the Fe-rich nanocrystals tend to diffuse towards the surrounding amorphous matrix, thereby increasing the thermal stability of the matrix and shifting the second crystallization reaction to higher temperatures.[20] As a result, the observed simultaneous crystallization of both the Fe_3Si and Fe-B compound phases during CA has been effectively separated during RA. The extent of separation depends on the rate at which the Nb concentration increases in the amorphous matrix. Furthermore, the reduced crystallite sizes (∼15 nm) observed during RA is a result of both, the Nb pile-up at the nanocrystal interfaces and the reduced annealing duration (10 s) imposed during RA. It is well known that Nb is effective in retarding the grain growth of Fe-Si nanocrystals. Hence, the observed pile-up of Nb (in Fig. 4(a)) further assists in controlling the growth rate of nanocrystals. In this way, a homogeneous nucleation dominated nanocrystallization process is realized in the amorphous matrix rather than an extended growth of already nucleated nanocrystals prevalent during CA.[5] As a result, formation of a high number density of smaller sized Fe_3Si nanocrystals in the amorphous matrix was achieved upon RA. At the same time, the crystallization of the residual amorphous matrix into complex Fe-B compound phases is suppressed. Hence, a large scale magnetic domain structure as well as corresponding low coercive fields leads to the soft-magnetic nature of the Cu-free alloy. In this way, similar nanocomposite microstructures comparable to that of Cu-containing alloys have been realized by RA of Cu-free $Fe_{74.5}Si_{15.5}Nb_3B_7$ alloy, demonstrating the effectiveness of RA in phase selection and nanostructure optimization for future soft magnetic materials.

IV. CONCLUSIONS

The nanocrystallization kinetics of Cu-free $Fe_{74.5}Si_{15.5}Nb_3B_7$ alloy on RA and CA was investigated, and the following conclusions are drawn:

(1) RA overcomes conventional limitations in realizing soft-magnetic nanostructures in Cu-free $Fe_{74.5}Si_{15.5}Nb_3B_7$ amorphous alloy.
(2) By employing RA isolated nucleation of Fe_3Si nanocrystals was achieved, while the formation of Fe-B compound phases was suppressed in the amorphous matrix.
(3) The mobility of Nb is especially critical for nucleation and growth of the Fe-Si phase. Upon RA, the diffusion of Nb atoms in the amorphous matrix is enhanced by at least two orders of magnitude resulting in increased nucleation rates. Crystal growth, however, is drastically limited by the reduced annealing duration of 10 s during RA.
(4) The resulting nanostructure upon RA is fully soft-magnetic with Hc ∼ 10 A/m and Js ∼ 1.2 T. However, the achieved maximum Fe-Si volume fraction is limited (to ∼40 vol. %) which is about 50% lower than that of the optimum Cu-containing $Fe_{73.5}Si_{15.5}Nb_3B_7Cu_1$ alloy.

[1]G. Herzer, Acta Mater. **61**, 718 (2013).
[2]Y. Yoshizawa, S. Oguma, and K. Yamauchi, J. Appl. Phys. **64**, 6044 (1988).
[3]G. Herzer, *Handbook of Magnetic Materials* (Elsevier, Amsterdam, 1997), Vol. 10.
[4]K. Hono, D. H. Ping, M. Ohnuma, and H. Onodera, Acta Mater. **47**, 997 (1999).
[5]K. G. Pradeep, G. Herzer, P. Choi, and D. Raabe, Acta Mater. **68**, 295 (2014).
[6]K. Hono, Prog. Mater. Sci. **47**, 621 (2002).
[7]G. Herzer, V. Budinsky, and C. Polak, Phys. Status Solidi B **248**, 2382 (2011).
[8]K. Hono and D. H. Ping, Mater. Charact. **44**, 203 (2000).
[9]P. Sharma, X. Zhang, Y. Zhang, and A. Makino, Scr. Mater. **95**, 3 (2015).
[10]E. V. Voronina, N. V. Ershov, A. L. Ageev, and Y. A. Babanov, Phys. Status Solidi B **160**, 625 (1990).
[11]M. De Graef, M. A. Willard, D. E. Laughlin, and M. E. McHenry, IEEE Trans. Magn. **37**, 2343 (2001).
[12]Z. Akase, S. Aizawa, D. Shindo, P. Sharma, and A. Makino, J. Magn. Magn. Mater. **375**, 10 (2015).
[13]G. Rixecker, P. Schaaf, and U. Gonser, Phys. Status Solidi A **139**, 309 (1993).
[14]A. K. Arzhnikov, L. V. Dobysheva, G. N. Konygin, E. V. Voronina, and E. P. Yelsukov, Phys. Rev. B **65**, 024419 (2002).
[15]K. G. Pradeep, G. Herzer, and D. Raabe, Ultramicroscopy **159**, 285 (2015).
[16]F. C. Frank, Proc. Roy. Soc. A **201**, 586 (1950).
[17]D. R. Allen, J. C. Foley, and J. H. Perepezko, Acta Mater. **46**, 431 (1998).
[18]J. C. Foley, D. R. Allen, and J. H. Perepezko, Scr. Mater. **35**, 655 (1996).
[19]J. Geise and C. Herzig, Z. Metallkd. **76**, 622 (1985).
[20]U. Köster, Key Eng. Mater. **81–83**, 647–662 (1993).
[21]U. Köster, U. Schünemann, M. Blank-Bewersdorff, S. Brauer, M. Sutton, and G. B. Stephenson, Mater. Sci. Eng. A **133**, 611 (1991).
[22]K. G. Pradeep, Ph.D. Dissertation, Shaker Verlag GmbH, 2014. ISBN: 978-3-8440-3211-6.

RIGHTSLINK